Journal of Sound and Vibration 486 (2020) 115619

Contents lists available at ScienceDirect

Journal of Sound and Vibration

journal homepage: www.elsevier.com/locate/jsv

An alternative and optimized thickness profile of an acoustic black hole plate

Li Ma, Hao-Wen Dong, Li Cheng*

Department of Mechanical Engineering, The Hong Kong Polytechnic University, Hong Kong

ARTICLE INFO

Article history:
Received 3 February 2020
Revised 20 June 2020
Accepted 2 August 2020
Available online 4 August 2020

Keywords:
Acoustic Black Hole (ABH) plate
Thickness profile
Optimization
ABH local modes
Vibration and sound radiation

ABSTRACT

Owing to their unique wave retarding features, Acoustic Black Hole (ABH) structures with standard power-law thickness profiles have been extensively explored for various structural vibration and sound radiation control applications. In order to achieve even better ABH effects for a given minimum thickness that can be achieved or accepted in practice, this paper reports an alternative ABH thickness profile in a plate through an optimization procedure by using the fast and elitist nondominated sorting genetic algorithm II in conjunction with a 2D semi-analytical Daubechies wavelet model. The new thickness profile features a different geometry from the standard ones in that the position of the imposed minimum thickness is off-set from the ABH indentation center, thus forming a flexible ring-shaped area and creating bi-directional ABH effects, which is conducive to energy focusing and dissipation. Numerical results show that a plate embedded with the optimized ABH indentation exhibits better ABH effects than its standard ABH counterpart, as evidenced by an increase in the total system damping as well as an impairment of other vibration and sound radiation metrics. Mode shape analyses of the optimized ABH plate show that the observed damping increase is mainly attributed to these local ($\bar{n}$, 1) and ($\bar{n}$, 2) modes, as a result of the flexible ring-shaped area that is formed inside the optimized ABH indentation. Finally, the optimized ABH plate is shown to entail reductions in both the vibration response of the plate and its sound radiation into a free acoustic medium.

1. Introduction

As a passive, efficient and promising technique for vibration control and sound radiation mitigation, structures embracing acoustic black hole (ABH) principles have attracted increasing attention during the last three decades. For thin-walled structures with decreasing thickness according to a power-law relationship, the phase velocity of propagating waves travelling through such structures would slow down alongside a drastically amplified vibration amplitude, leading to efficient energy focusing and dissipation if the thin area is covered with a small amount of damping material. This phenomenon is the so-called Acoustic Black Hole effect [1], whose process is a combination of the thickness-induced wave retarding/focusing and damping-induced energy dissipation. Apart from the standard power-law thickness profile, structures having other thickness profiles, as long as the basic thickness-induced wave retarding/focusing phenomenon is preserved, can also be referred to as ABH structures in a broader sense [2,3]. These unique features entail remarkable energy focusing within the central area

* Corresponding author.
E-mail address: li.cheng@polyu.edu.hk (L. Cheng).

https://doi.org/10.1016/j.jsv.2020.115619
0022-460X/

of the indentation and allow for effective energy dissipation with the use of a small amount of damping material, thus resulting in significant reductions in both structural vibration [2,4–6] and sound radiation [7–10].

ABH effects are strongly dependent on the thickness profile. The pioneer work of Mironov established the fact that this can be readily achieved with a standard power-law thickness profile when the exponent is equal to or larger than two [11]. Since then, such a standard profile has been widely adopted by a large amount of research work to investigate various issues pertinent to ABH phenomena. As a persistent effort to enhance the ABH effects and to increase their practical applicability, efforts have also been devoted to investigating issues arising from slight geometrical variations of the ideal standard ABH profile. Taking a one-dimensional ABH beam as an example, previous analyses showed that the truncation thickness at the taper end, the length and the power law index of the ABH taper, and the coverage of the add-on damping layers all have great influence on the ABH effects. More specifically, Tang et al. investigated the effect of the truncation thickness [12] and that of the extended platform [13] on the vibration response and the modal loss factors of an Euler-Bernoulli beam, respectively. Krylov and Tilman [14] examined the reflection coefficients of flexural waves from the edges of a standard ABH structure with different power law indices. Their results showed that a smaller truncation thickness and a larger power law index would warrant better ABH effects. Also, Denis et al. [1] used a Kundt-like method to experimentally measure the reflection coefficient of an ABH beam. The results showed that the reflection coefficient was of the same order of magnitude up to 4000 Hz compared with that obtained by the impedance matrix method [15,16]. The differences in the reflection coefficient above 4000 Hz were attributed to the geometrical imperfections of the experimental sample. In addition, the add-on damping layer over the ABH indentation surface also plays an important role. Investigations showed that a moderate amount of damping material coated at the central portion of an ABH indentation in a plate would lead to effective energy dissipation [8,12], and that excessive use of damping material would possibly impair the energy focusing [8] and jeopardize the expected sound radiation reduction of ABH structures [17]. Meanwhile, Huang et al. [3] investigated a plate with a so-called imperfect ABH indentation for better wave focusing effect. The indentation thickness geometry differs from the conventional one in that a uniform base was added to the standard thickness profile. Along the same line, Huang et al. [18]. topologically optimized the material parameters of the damping layer over an ABH surface to maximize the viscous dissipation. Hook et al. [19] parametrically studied the influence of the truncation thickness, taper length, and power law on broadband reflection coefficients of an ABH beam. McCormick and Shepherd [20] used an multi-objective approach to investigate three types of ABH vibration absorbers.

It can be seen that nearly all existing work adopted either the standard or slightly varied power-law thickness profiles with the thinnest part being located either at the tip end in one-dimensional cases or the center of the indentation in two-dimensional cases. Therefore, the open question is whether it is possible to obtain alternative ABH profiles which warrant better ABH effects while satisfying the prescribed thickness constraints imposed by the existing manufacturing capability. This is obviously a structural optimization problem under the umbrella of the ABH. As far as we know, the search for alternative ABH profiles which are significantly different from the standard ones through optimization has not been reported in the open literature up to now. This motivates the present work.

Therefore, this paper targets a dual-objective: 1). to propose an alternative ABH thickness profile which would mainly depend on structural thickness changes through a systematic optimization, which ultimately warrants the best possible ABH effects under a prescribed minimum thickness constraint; and 2). to demonstrate the enhanced ABH features through the exploration of the underlying physics in relation to the new thickness geometry. The reported study shall lead to a new ABH thickness profile which is, in principle, different from the classical ABH profiles defined by the standard power-law relationship.

The task is challenging which requires two important and indispensable components: a physical solver and an optimizer. For the former, a versatile and flexible structural model is a pre-requisite to simulate and capture the fine details of the structural dynamics when the thickness profile evolves. It is relevant to mention that most of existing ABH studies in the literature use finite element models which are indeed convenient to handle structures of complex geometries. However, with the compressed wavelength inside the ABH area, denser element meshes are needed to capture the local structural details, thus leading to intensive computation time in each optimization loop. To tackle the problem, a previously developed semi-analytical Daubechies wavelet (DW) model [9,21] is used and integrated into an optimization procedure. Capitalizing on its flexibility and efficiency, we use the model to simulate the vibrational and acoustic responses of an ABH plate with a general ABH thickness profile characterized by a polynomial with its power indices up to four to satisfy the smoothness conditions [14,19,22]. To perform the optimization, a fast and elitist genetic algorithm: Nondominated Sorting Genetic Algorithm II (NSGA-II) is used. The overall structural damping, which is independent from external excitations, is taken as an intrinsic indicator to evaluate the overall ABH effects. More specifically, the sum of the first one hundred modal loss factors of the ABH plate is taken as the objective function which will be maximized by the adopted optimizer.

The rest of this paper is organized as follows. In Section 2, the description of the Lagrange interpolation polynomials is first introduced for the generation of the thickness profiles. The optimization problem is then defined, and the procedure of a constraint-handling NSGA-II and the DW model employed for the optimization are briefly described. In Section 3, the optimization is performed and an alternative ABH thickness profile is achieved. The robustness of the optimized ABH thickness profile is then evaluated. Numerical analyses of a clamped rectangular plate embedded with the optimized ABH indentation are then conducted. Issues relating to the optimized ABH profile such as the system loss factors, their relationships with modal deformation depicted by mode shapes, energy distribution as well as vibration and sound radiation properties are scrutinized. In addition, the vibration response of the optimized ABH plate is analyzed through wavenumber transform to

explain the improved ABH effect resulting from the optimized ABH profile. Results are also compared with those of standard ABH plates with the same maximum taper power index of four. Finally, a summary is given in Section 4.

2. Problem statement and optimization procedure

In this section, the creation of ABH thickness profiles and the optimization procedure are described. We investigate a rectangular plate with an embedded circular ABH indentation. The indentation portion is formed by rotating a curved line around one of its ends which is fixed to an axis (z axis) normal to the plate (see Fig. 1). The curved line, obtained by cutting through the center of the indentation and taking only half portion of the profile, is the one-dimensional thickness profile that is to be optimized hereafter. The optimization problem is defined below alongside a brief recap of the NSGA-II and the DW model used for optimization.

2.1. Lagrange interpolation polynomials for profile generation

We first discuss the description of the thickness profile. We use Lagrange interpolation polynomials because they can uniformly approximate any continuous functions defined within a bound. Assuming $\tilde{n}$+1 distinct data points at $x_0, x_1, \cdots x_{\tilde{n}}$, and $\tilde{f}$ as a function whose values are given at these points, there exists a unique polynomial $P(x)$ of degree at most $\tilde{n}$ with

$$\tilde{f}(x_k) = P(x_k) \tag{1}$$

in which $k = 0, 1, 2, \ldots, \tilde{n}$. The polynomial is given by

$$P(x) = \sum_{k=0}^{\tilde{n}} \tilde{f}(x_k) l_k \tag{2}$$

where l_k is the Lagrange interpolation operator, written as

$$l_k = \prod_{\substack{j=0 \\ j\neq k}}^{\tilde{n}} \left(\frac{x - x_j}{x_k - x_j} \right) \tag{3}$$

The Lagrange interpolation polynomial is used to create the thickness profile for each individual in the population during the optimization process. For the convenience of illustration, the origin of the coordinate system is transformed to the ABH center. In the present case, five distinct points, $(0,z_1)$, $(x'_{\min},h_0)$, (x'_2,z_2), (x'_3,z_3) and (R_{ABH}, h) as shown in Fig. 2, are used to depict the 1D half ABH thickness profile as defined before. Therefore, the largest total number of terms in the profile expressions is five. The choice is made to satisfy the smoothness condition required for the realization of ABH effect, since the order of the standard power-law thickness profile is usually chosen between 2 and 4, which can be readily achieved by standard CNC milling. To define the searching scope, the diameter of the ABH indentation ($2R_{ABH}$), the minimum thickness h_0 and the maximum thickness h of the thickness profiles, which is the same as the uniform portion of the plate, are given *a priori* and kept constant. The thickness at the junction between the uniform portion of the plate and the ABH outer boundary should be continuous, *i.e.*, the point (R_{ABH}, h) is also given *a priori*. The x' coordinates of the points in the transformed coordinate for creating the polynomials in Eq. (2) are uniformly distributed. In the current case, $x'_2 = 1/3R_{ABH}$ and

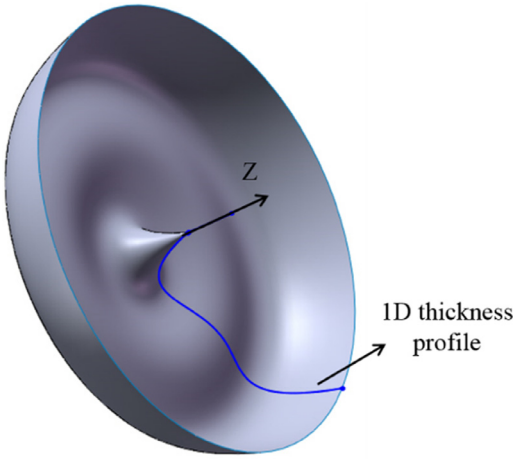

Fig. 1. Schematic of a 2D circular indentation formed by rotation of a 1D thickness profile around z axis. This ABH element is to be embedded into a rectangular plate to form an ABH plate.

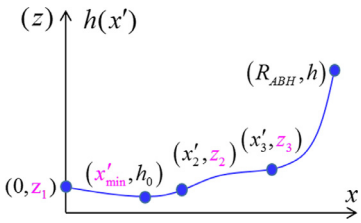

Fig. 2. The distinct points that determines the ABH thickness profile. Design variables are shown in pink color.

$x'_3 = 2/3R_{ABH}$, and the corresponding thickness z_2, z_3, and z_1 at the indentation center are to be determined. The minimum thickness of the ABH profiles is set to be h_0=0.6 mm, for both the standard ABH profile and the optimized ABH profile. However, the position of the minimum thickness, $x'_{\min}$, is not fixed *a priori*. As a result, there are four design variables: the thickness z_1 at the indentation center, the thicknesses z_2 and z_3 at two fixed x'coordinates and the position of the minimum thickness, $x'_{\min}$. The variable bounds for z_1, z_2, z_3 and $x'_{\min}$ are $[h_0, h]$ and $[0, R_{ABH})$, respectively.

The above profile description allows for generating various thickness profiles during the optimization process, including the initial population containing multiple individuals which are randomly generated in compliance with Eq. (2) to start the optimization process. The corresponding 2D circular indentations are expressed as $h(r) = a_0 + a_1 r + a_2 r^2 + \cdots + a_\gamma r^\gamma$, where a_0, a_1, a_2 and a_γ are the coefficients of the polynomial, and $\gamma = 4$.

2.2. Objective function and constraints

The optimal ABH thickness profile under search is supposed to provide improved overall ABH effects as compared to its counterpart with a standard thickness profile. As a quantitative measure, the overall structural damping is used to construct the objective function to be used in the optimization. More specifically, the sum of the first one-hundred modal loss factors of the plate is maximized. As can be seen at later sections, this can properly cover the frequency range within which optimizations are performed. Unlike other vibration metrics such as forced vibration response, damping loss factors are independent of the external excitation. That is why they are chosen here to construct the objective function in order to reduce the reliance of the optimized profile on other parameters such as excitation.

To assess the structural damping increase with the alternative profiles, a standard ABH plate, with $h(r) = \varepsilon r^\gamma + h_0$, is used for comparisons, in which ε is a constant, γ the power law index, r the distance from the ABH center and h_0 the minimum thickness of the ABH, which is kept the same as the optimized one.

In this optimization problem, the fitness function is defined as the reciprocal of the objective function, which will be minimized. The problem is mathematically defined as

$$\begin{aligned} & fitness = \frac{1}{\sum_{i=1}^{100} \eta_i} \\ \text{s.t.} \quad & h_0 \le h(x') \le h \\ & 0 \le x'_{\min} < R_{ABH} \\ & \int_0^{R_{ABH}} k_{opt}(x')dx' > \int_0^{R_{ABH}} k_{std}(x')dx' \end{aligned} \tag{4}$$

in which η_i stands for the modal loss factor of the i^{th} mode of the ABH plate; k_{opt} and k_{std} are the real parts of the wavenumbers of the flexural waves inside the ABH indentations of the optimized profile and the standard profile, respectively. The first constraint $h_0 \le h(x') \le h$ defines the variation range of the thickness of the profiles. The second constraint $0 \le x'_{\min} < R_{ABH}$ stipulates that the position of the minimum thickness can be anywhere within the indentation, rather than fixed at the indentation center as in the case of a standard ABH indentation. The most salient feature of the ABH phenomenon is the gradually reducing phase velocity and energy focalization of flexural waves. The last constraint $\int_0^{R_{ABH}} k_{opt}(x')dx' > \int_0^{R_{ABH}} k_{std}(x')dx'$ ensures that the accumulated phase of the flexural waves travelling inside the optimized ABH indentation is larger than that inside the standard indentation, which imposes that propagating waves would take more time to travel inside the optimized indentation. This way, we make sure that the finally obtained profile preserves the basic features of the ABH so that it can be called an ABH profile. Note this last constraint is crucial to ensure that the optimized structure inherits the basic ABH features and outperforms the conventional one with standard ABH profile from the wave propagation viewpoint. In the present case, the integration on the left side of the last constraint in Eq. (4) is discretized as $\int_0^{R_{ABH}} k_{opt}(x')dx' = \sum_{i=1}^{N} k_{opt,i}(x'_i)\Delta x'$during the calculation, where $N = 200$ and $\Delta x' = \frac{R_{ABH}}{N}$. The other integration terms on the right-hand side of the last constraint is treated similarly.

2.3. Physical modelling

A physical model is needed to feed the optimization process. The model should be versatile, flexible and efficient enough to accommodate thickness profiles of arbitrary shape. In addition, the model should be able to consider the full coupling

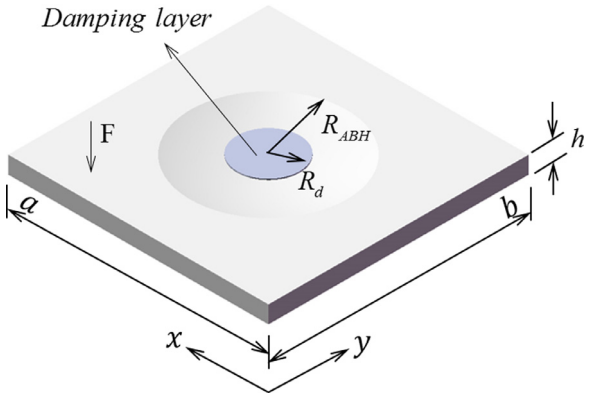

Fig. 3. A rectangular plate embedded with a circular indentation partially coated with damping layer.

between the indentation and the add-on damping layer in a flexible manner. In the present case, a previously developed 2D Daubechies wavelet (DW) model [9,21] is utilized to simulate the dynamic behavior of an ABH plate for both optimization and further performance evaluation. As illustrated in Fig. 3(a), the model consists of a plate (with the dimensions $a \times b$) embedded with a circular indentation of any thickness variation (symmetrical standard power-law or a general profile described by polynomials generated in Section 2.1), and symmetrically coated by damping layers on both sides. The circular ABH indentation has a radius of R_{ABH}, centered at (x_c, y_c). The add-on damping layer is modelled as an integral part of the system. Both its mass and the stiffness are included in the model and fully coupled with the plate [21].

The DW model is based on the Love-Kirchhoff thin plate theory which assumes that the system is symmetrical with respect to its midplane. Employing dimensionless coordinates $\xi = x/a$ and $\eta = y/b$, the transverse displacement w is approximated by

$$w = \sum_{i}^{\bar{p}} \sum_{j}^{\bar{q}} a_{ij}(t)\varphi_i(\xi)\varphi_j(\eta) \tag{5}$$

in which $\varphi_i(\xi)$ and $\varphi_j(\eta)$, utilized as admissible functions, are Daubechies wavelet scaling functions in x and y directions, respectively; $\bar{p}$ and $\bar{q}$ are the truncation orders representing the number of terms of admissible functions to be used in the computation [21]; $a_{ij}(t)$ are the unknown complex coefficients which are also the generalized coordinates in the Euler-Lagrange equations resulting from the stationary state of the system. Subsequently, the equation of motion for the system writes

$$\left(\mathbf{K} - \omega^2\mathbf{M}\right)\mathbf{A} = \mathbf{F} \tag{6}$$

where **M**and **K**represent the global mass and complex stiffness matrices, respectively. Expressions of **M** and **K** are described in detail in Ref. [21]. For free vibration analyses, the eigenvalue problem in Eq. (6) gives the complex natural angular frequencies as:

$$\omega^2 = \omega_n^2(1 + i\eta_n) \tag{7}$$

where ω_n is the undamped natural angular frequency and η_n the corresponding modal loss factor. η_n is a useful parameter to characterize the energy dissipation of each individual structural mode. Upon obtaining the solution of Eq. (6), the calculation procedures of the sound radiation field is straightforward as described in Ref. [9].

2.4. Optimizer: constraint-handling NSGA-II

NSGA-II, a fast and elitist genetic algorithm [23], is briefed here for the completeness of the paper. The procedure starts from the generation of a random population P_t of size N_p, with each individual being assigned a fitness value that is equal to its nondominant level. Then the following procedures are performed to minimize the fitness.

1) An offspring Q_t of the same size N_p is created through binary tournament selection, recombination and mutation operators.
2) Combining the parent population and the offspring leads to a combined population $\tilde{R}_t$ of size $2N_p$; this combination guarantees the elitism of the population.
3) Sorting the combined population $\tilde{R}_t$ using nondomination.
4) Assembling a new population P_{t+1} of size N_p.
5) Finally, the new population P_{t+1} will be used to create next generation, and the above steps will be repeated till the convergence of the fitness function.

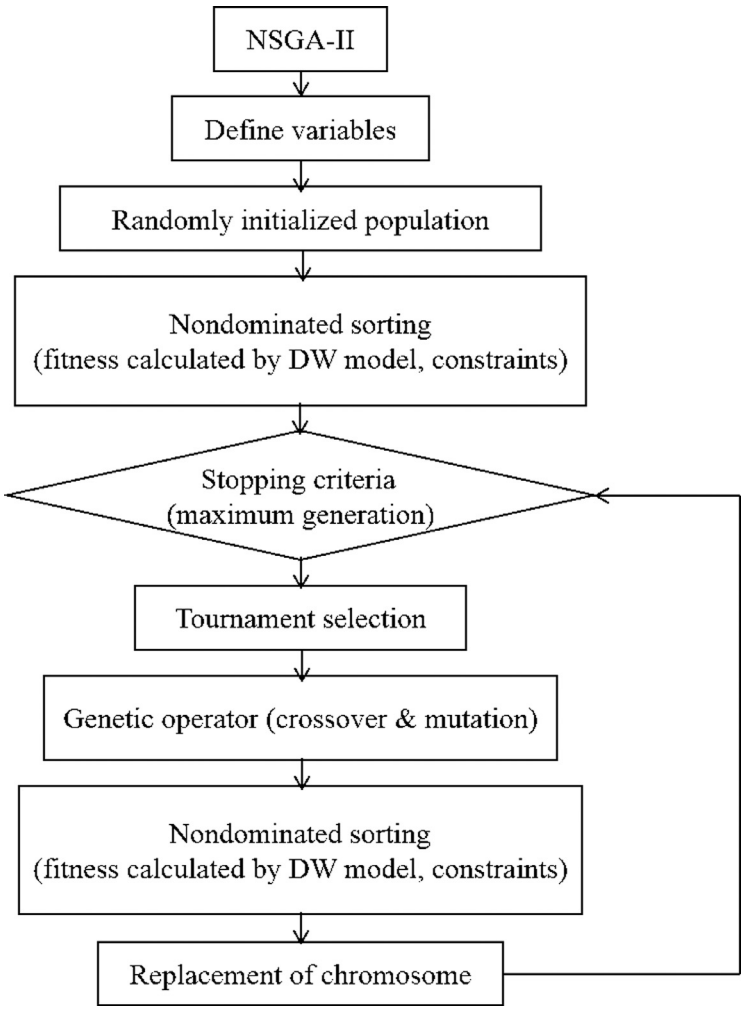

Fig. 4. The flowchart of NSGA-II.

The flowchart to get the converged optimal solution is shown in Fig. 4.

A strategy for handling constraints [23] is necessary for implementations. Algorithms based on tournament selection proves to be better than a number of other algorithms in this regard. The adopted constraint-handling approach uses the tournament selection, *i.e.*, two individuals are picked from the population and the best one is selected. Each individual can be feasible or infeasible in the presence of constraints. Considering the single objective optimization nature of the current problem, the following simple rule is used for the tournament selection:

1) If both individuals are feasible, the one with a better objective function will be chosen;
2) If one individual is feasible and the other one is not, choose the feasible one;
3) If none of the individuals is feasible, choose the one with smaller overall constraint violation.

3. Numerical analyses and discussions

3.1. Optimized thickness profile

Implementing the NSGA-II described above, the minimization problem defined in Eq. (4) is performed in conjunction with the DW model. The sum of the first 100 modal loss factors of a rectangular plate with an indentation of randomly generated profiles is maximized. The edges of the plate are clamped, which are achieved using artificial springs [21]. The geometrical parameters of the standard ABH plate are tabulated in Table 1. The material parameters of the ABH plate and the add-on damping material F9473PC are shown in Table 2. As aforementioned, this study targets an alternative thickness profile that would mainly depend on structural thickness. Although simultaneous optimizations with different damping layouts are definitely possible, the optimized solution would be more case-dependent, especially on different damping layouts.

Table 1
Geometrical parameters of the standard ABH plate.

$a = 0.6$ m	$x_c = 0.3$ m	$\varepsilon = 10.67$/m
$b = 0.5$ m	$y_c = 0.25$ m	$\gamma = 4$
$h = 6$ mm	$h_0 = 0.6$ mm	$R_{ABH} = 0.15$ m

Table 2
Material parameters of ABH plates and the damping layer.

	Density	Elastic modulus	Loss factor	Poisson's ratio
ABH plate	$\rho_0 = 2800$ kg/m^3	$E_0 = 71$ GPa	$\eta_0 = 0.002$	$\nu_0 = 0.33$
F9473PC	$\rho_d = 980$ kg/m^3	$E_d = 30$ MPa	$\eta_d = 0.9$	$\nu_d = 0.499$

Therefore, to minimize the effects of the damping layer on the intrinsic thickness-dominant profile so as to achieve a more general and less case-specific profile, the parameters of the damping layer are *a priori* fixed. In the present case, the entire surface of the ABH indentations is covered with the soft damping material F9473PC produced by 3 M company. The Young's modulus of the damping material is as soft as 30 MPa to minimize the influence of damping layout on the thickness profile. The thickness of the damping material on each side of the indentation is 0.75 mm. h_0 is chosen to be 0.6 mm, that can be readily achieved through conventional manufacturing capability for metal structures (note the ABH profile is double-sided, which would increase the manufacturing difficulty). Meanwhile, this might also be the minimum thickness that can be acceptable for practical applications. A smaller h_0 is expected to lead to better performance.

Except for the thickness profiles inside the indentations, the plates with alternative profiles have the same dimensions, material parameters and damping configuration as the standard ABH plate.

In the optimization, the initial population is randomly generated. The differences in terms of four variables between two sets of randomly generated initial populations are shown in Table 3 below. It follows that inside a population, variables between individuals clearly show differences. In addition, individuals between these two sets of populations also show obvious differences. This demonstrates the diversity of the randomly generated individuals in the initial populations.

For the physical DW model, the supported length L and resolution m used in the wavelet series are selected to be 12 and 5, respectively. Distribution indices [24] are used for crossover and mutation operators as η_c=20 and η_m=20, respectively. The convergence is reached when the difference in the objective function between two consecutive steps is within 0.2% in a wide step interval. In the present case, after around 153 generations, the fitness function converges. For comparisons, the values of the objective function for the randomly generated initial population before optimization are presented in Fig. 5. Best values corresponding to the population in each optimization generation are shown in Fig. 6(a). Note an initial population containing 96 individuals are randomly generated in compliance with Eq. (2) to start the optimization process.

Fig. 6(a) shows that the value of the best individual in each generation experiences a rising trend with the increase of the generation number. Though most of the objective values for the initial population are relatively low (shown in Fig. 5),

Table 3
Distribution of four design variables of 96 individuals in different runs. Note the horizontal axis represents the number of individuals from 1 to 96, with color bar indicating the values of individual variables.

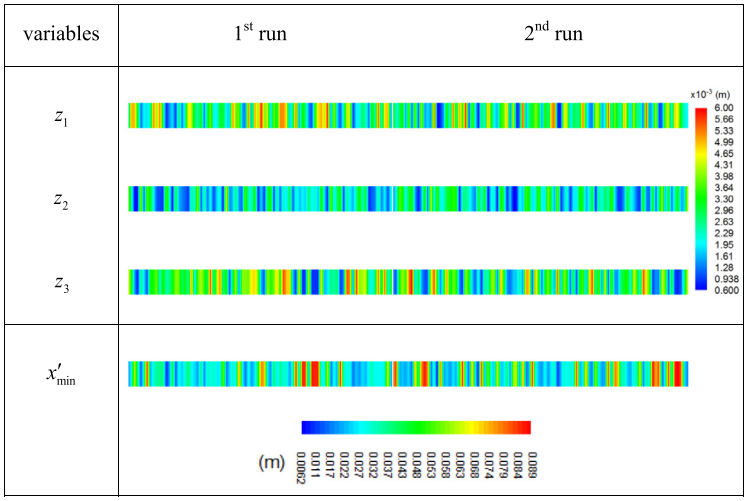

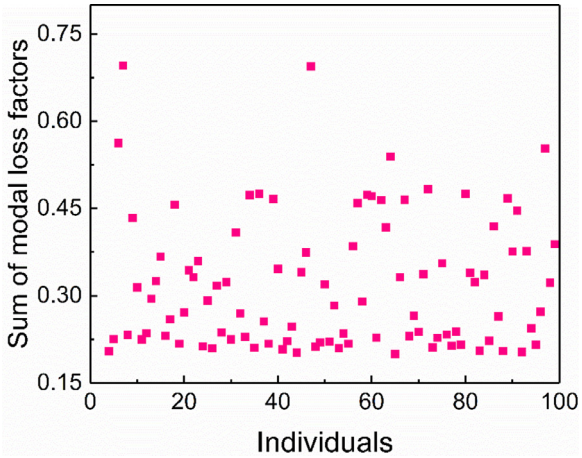

Fig. 5. Objective values for the initial population.

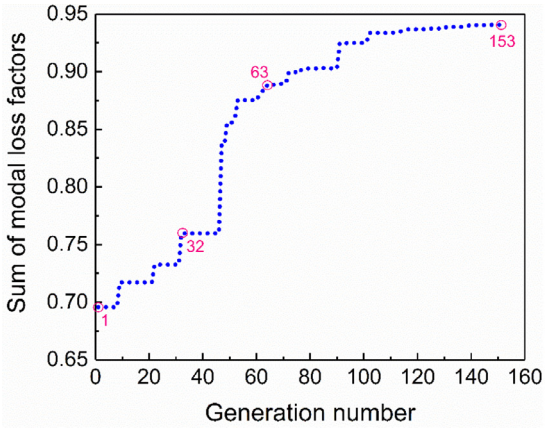

(a)

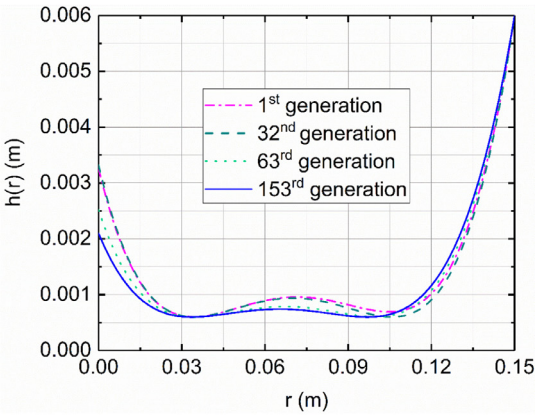

(b)

Fig. 6. Steps of the optimization process: (a) objective of the best individual in each generation; (b) optimal profile in specific generations: the 1st generation (dash dot line); the 32nd generation (dash line); the 63rd generation (dot line); the 153rd generation (solid line).

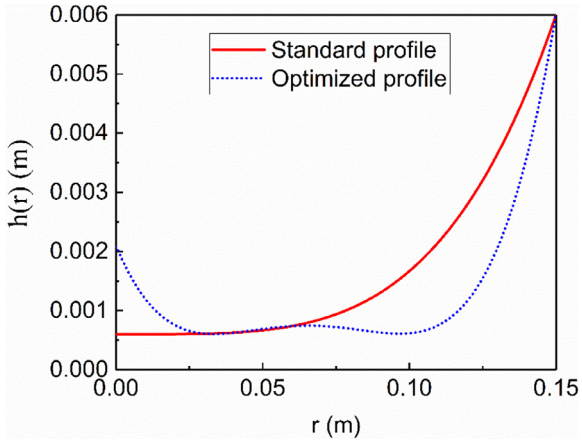

Fig. 7. The optimized profile and the standard profile in the radial direction.

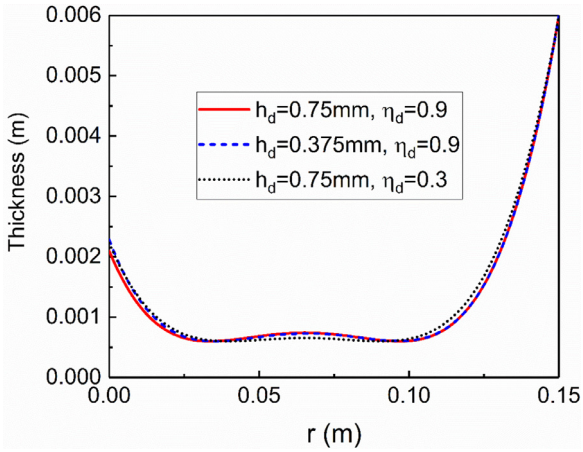

Fig. 8. Comparisons of optimized thickness profiles with damping layers of different thicknesses and loss factors: solid line: thickness 0.75 mm, loss factor 0.9; dash line: thickness 0.375 mm, loss factor 0.9; dot line: thickness 0.75 mm, loss factor 0.3.

the one with the largest value is actually very close to the final optimal one. To illustrate the evolution process, profiles of the best individuals at several generation steps (1st, 32nd, 63rd, 153rd) are illustrated in Fig. 6(b). It can be seen that portion of the thickness profiles which is close to the outer junction with the uniform part of the plate gradually reduces (from 1st to 32nd generation) and then becomes thicker (from 32nd to 153rd generation), while other parts of the profiles show a decreasing trend with the increase of the generation number. Finally, the optimization result converges to the best individual without noticeable further changes.

The ultimate ABH thickness profile, described in a polar coordinate system gives: $h_{opt}=(0.0021)+(-0.12)r+(3.3243)r^2+(-36.85)r^3+141.23r^4$ in the circular coordinate system. Its corresponding counterpart of a standard thickness profile, with $h_{std}=(0.6e-3)+10.67r^4$, is used for comparisons. Fig. 7 shows both profiles in 1D view in the radial direction of the indentation. Different from the standard profile, the optimized one undergoes a sharp decrease in thickness when entering into the ABH indentation from the outer junction with the uniform part of the plate, dwells into a thin plateau and then undergoes a raise-up at the indentation center. The panel thickness at the ABH center is around 2.1 mm. The position of the minimum thickness is 0.0336 m away from the indentation center in the radial direction.

3.2. Robustness of the optimized thickness profile

To evaluate the effectiveness and the robustness of the optimized profile, optimizations are repeated for two additional cases. In the first case, the thickness of the damping layer is halved with other parameters being kept the same. In the second case, a significantly different loss factor of the damping material (0.3 instead of 0.9) is used. After optimizations, the obtained profiles are compared with the standard configuration, as shown in Fig. 8. It follows that, despite some tiny differences, the optimized profiles in these three different cases are very similar, at least from engineering application viewpoint. This confirms the robustness of the optimization and the general character of the profile obtained. This is also consistent with the pre-set target to seek a different ABH profile, which would mainly depend on structural thickness changes instead

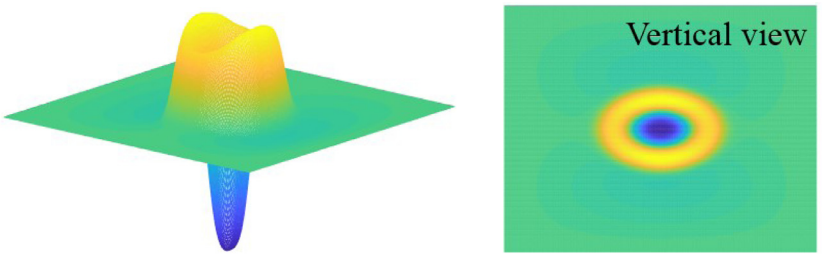

(a) 9th mode (modal loss factor 0.0124)

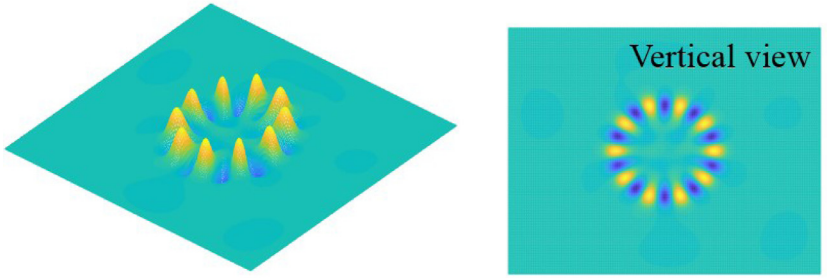

(b) 67th mode (modal loss factor 0.0151)

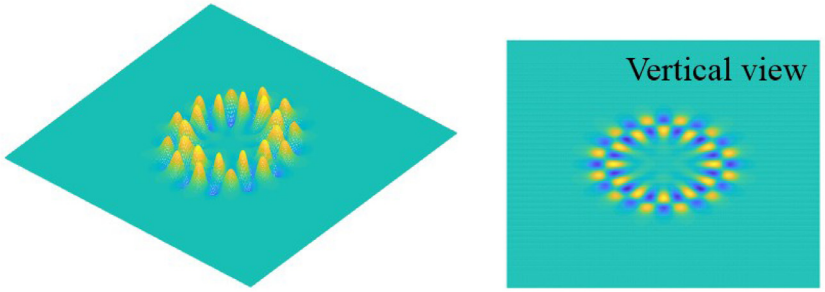

(c) 148th mode (modal loss factor 0.0141)

Fig. 9. Mode shapes of a plate embedded with an indentation of optimized ABH profile: (a) the 9th mode; (b) the 67th mode; (c) the 148th mode.

of other system parameters. This claim will be further substantiated by the numerical analyses on typical ABH features exhibited by the obtained profile, to be discussed in the following sections.

3.3. Structural features and damping performance

Numerical analyses on the optimized plate and the standard ABH plate are conducted. Firstly, mode shapes of the optimized plate are investigated. Several typical mode shapes (*i.e.*, 9th, 67th, 148th) representing low to high orders are presented in Fig. 9. It can be observed that, ABH local modes occur at relatively low orders such as the 9th mode. Similar phenomena can also be observed for the standard ABH plate. However, local ABH ($\bar{n}$, 1) and ($\bar{n}$, 2) modes inside the optimized ABH indentation are clearly observed at relatively high order modes, *e.g.* the 67th and 148th mode shapes, respectively, in Fig. 9(b) and Fig. 9(c). The ABH ($\bar{n}$, 1) and ($\bar{n}$, 2) modes herein represent the mode shapes that exhibit $\bar{n}$ half waves in the circumferential direction and one or two half waves in the radial direction of the indentation.

An examination on the modal loss factors shows that, the optimized ABH profile leads to an increase in the structural damping compared with the standard ABH profile. More specifically, the overall damping enhancement for the first 100 modes amounts to around 39.5%.

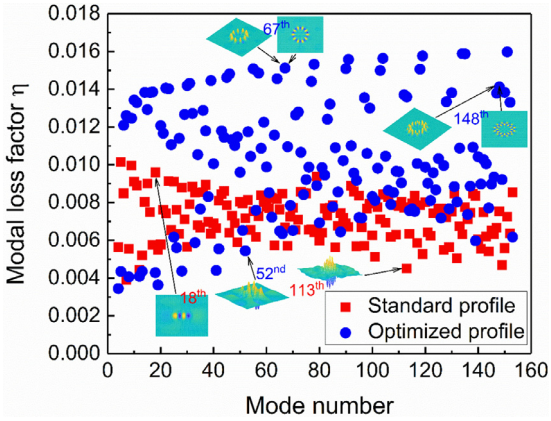

Fig. 10. Comparison of modal loss factors: (a) standard ABH plate (square dot); (b) optimized ABH plate (circular dot).

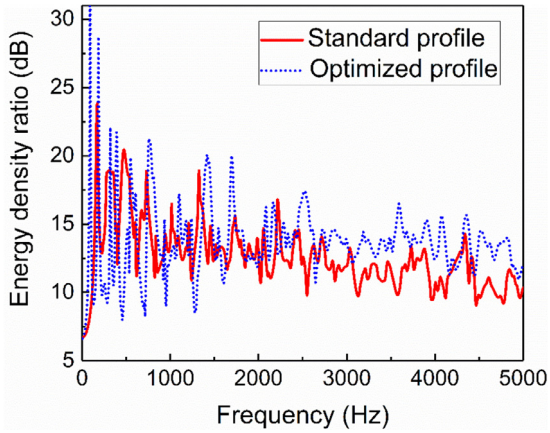

Fig. 11. Energy density ratio between the ABH portion and the uniform portion: (a) standard ABH plate (solid line); (b) optimized ABH plate (dot line).

To gain better insights into the underlying phenomena induced by the optimized profile, the first 150 modal loss factors of the standard ABH plate and those of the optimized ABH plate are illustrated in Fig. 10. Note that the last 50 modes were not directly involved in the optimization. The reason why they are being checked is to confirm the extended effects of the optimized ABH profile. It can be seen that, for the standard ABH plate, loss factors dwell in the interval (0.004, 0.01). For the optimized case, loss factors are primarily scattered from 0.004 to 0.016, with an average increase of roughly 43.7%, compared with those of the standard ABH plate. Typical mode shapes corresponding to loss factors of low, medium and high levels are also presented. Similar to the standard ABH plate, it seems that the low-value loss factors mostly correspond to the global modes, *e.g.* the 52nd mode for the optimized ABH plate and the 113th mode for the standard ABH plate, as shown in Fig. 10; in agreement with the analyses on the modal loss factors reported before [21]. For the standard ABH plate, the high-valued loss factors are mainly associated with ABH (1, 2), (2, 1), (1, 4) and (4, 1) modes, exemplified by the 18th mode shown in Fig. 10. The relationships between the modal loss factors and the modal deformation are similar to those for another standard ABH plate with power law index of 2 in Ref. [21]. Differently and interestingly, for the optimized ABH plate, the relatively high-value loss factors primarily correspond to ABH local ($\bar{n}$, 1) and ($\bar{n}$, 2) modes, *e.g.*, the 67th and 148th mode shapes shown in Fig. 9 and Fig. 10.

The occurrence of the local ABH ($\bar{n}$, 1) and ($\bar{n}$, 2) modes which exhibit high loss factors in the optimized ABH plate can be attributed to the unique feature of the optimized thickness profile. In fact, with the minimum thickness being offset from the indentation center, a ring-shaped area/plateau (from radius 0.0336 m to 0.0972 m in the present case) inside the indentation is formed, which reduces the structural stiffness around the circumferential direction and further promote energy focusing. For the standard ABH plate, however, only the central area of the indentation is effective in energy focusing. From wave propagation perspective, it can be surmised that the extended thin thickness plateau between the center and the outer boundary of the optimized ABH indentation (or the valley area of the ring) is believed to create bi-directional ABH effects so that wave energy can be trapped from both sides (inbound waves from the outer boundary of the indentation and the residual outbound waves reflected back from the indentation center). This physical process is conducive to enhancing energy focusing and dissipation, consequently the overall ABH effects.

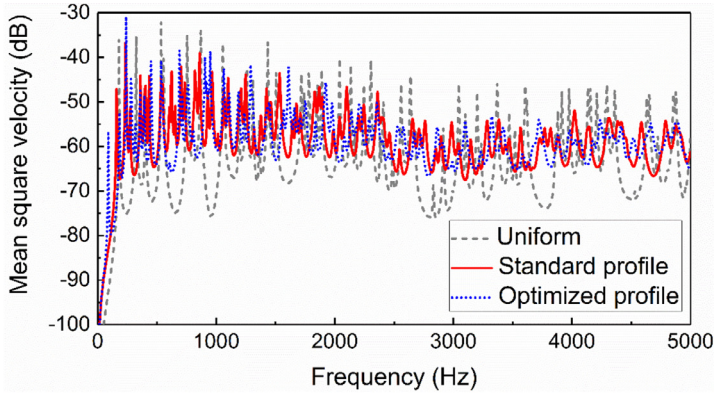

(a)

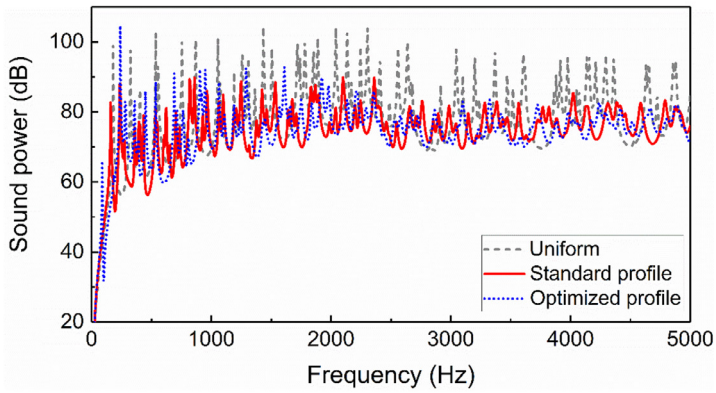

(b)

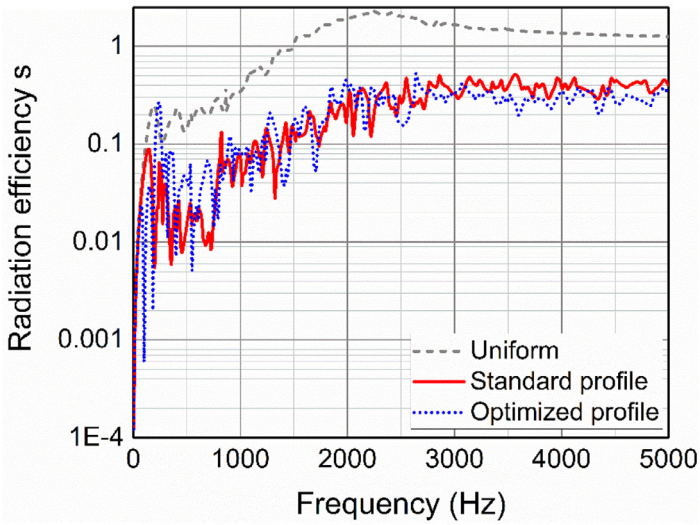

(c)

Fig. 12. Comparisons between a uniform plate (dash line), a standard ABH plate (solid line) and an optimized ABH plate (dot line): (a) space-averaged mean square velocity; (b) radiated sound power; (c) sound radiation efficiency.

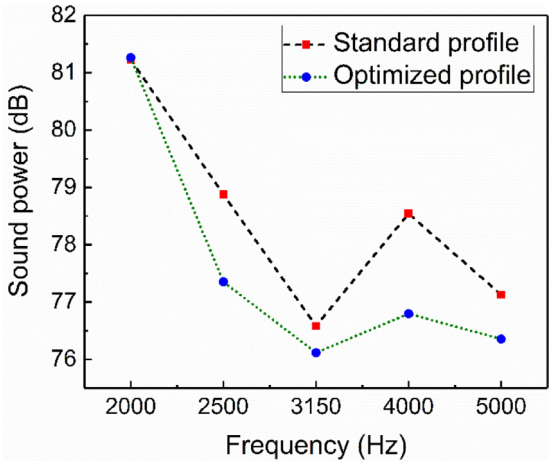

(a)

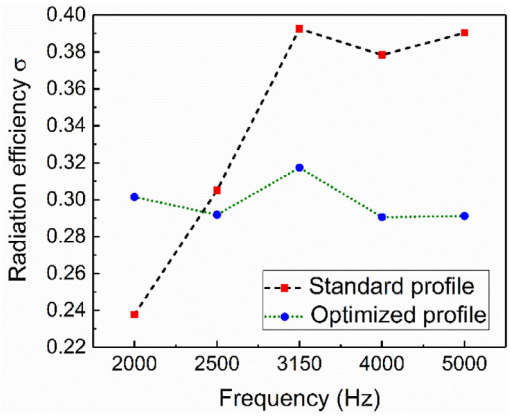

(b)

Fig. 13. Comparisons between the standard ABH plate and the optimized ABH plate in one third octave band: (a) radiated sound power; (b) sound radiation efficiency.

3.4. Performance verification in vibration and sound radiation reductions

To assess the energy focusing ability of the optimized ABH plate, an energy density ratio between the ABH portion and the uniform portion of the plate, defined as $10\lg[(\frac{1}{V_{ABH}}\int_{V_{ABH}}\mathbf{V}\mathbf{V}^{*}dV)/(\frac{1}{V_{uni}}\int_{V_{uni}}\mathbf{V}\mathbf{V}^{*}dV)]$, is assessed. Here, $\mathbf{V}$ is the complex velocity vector of the vibrating plate; V_{ABH} and $V_{uni.}$ are the volume of the ABH portion and the uniform portion, respectively.

In this case, a harmonic point force excitation is applied at (0.518, 0.165) m on the uniform portion of the plate. Comparisons between the standard ABH plate and the optimized ABH plate are illustrated in Fig. 11. It should be noted that the first 100 modes used in the optimization basically cover a frequency range up to 2690 Hz. We deliberately extend the examination range to 5000 Hz to verify the performance of the optimized ABH profile in an extended frequency range. It can be seen from Fig. 11 that the optimized ABH plate exhibits a higher energy density ratio than the standard one. This indicates that the optimized profile indeed exhibits better energy focusing, as an additional evidence of the enhanced ABH effects.

Furthermore, the vibration and sound radiation characteristics of the optimized ABH plate are investigated and compared with those of the standard ABH plate, as shown in Fig. 12(a)-(c), in terms of the mean square velocity, radiated sound power and radiation efficiency, respectively. To facilitate the comparison, results for a uniform plate having the same dimensions and coated with the same damping layers are also included as reference.

Compared with the uniform plate, it is not surprising that both the standard and the optimized ABH plates show reductions in the mean square velocity, radiated sound power and radiation efficiency, especially above the cut-on frequency [7] of 644 Hz, as expected. Meanwhile, a reduction in the peak levels of the mean square velocity (roughly 1.7 dB), radiated sound power (2.5 dB) and the radiation efficiency of the optimized ABH plate is also observed above the critical frequency of 1995 Hz, in comparison with the standard ABH plate. Since the size of the indentation is fixed, the optimization does not

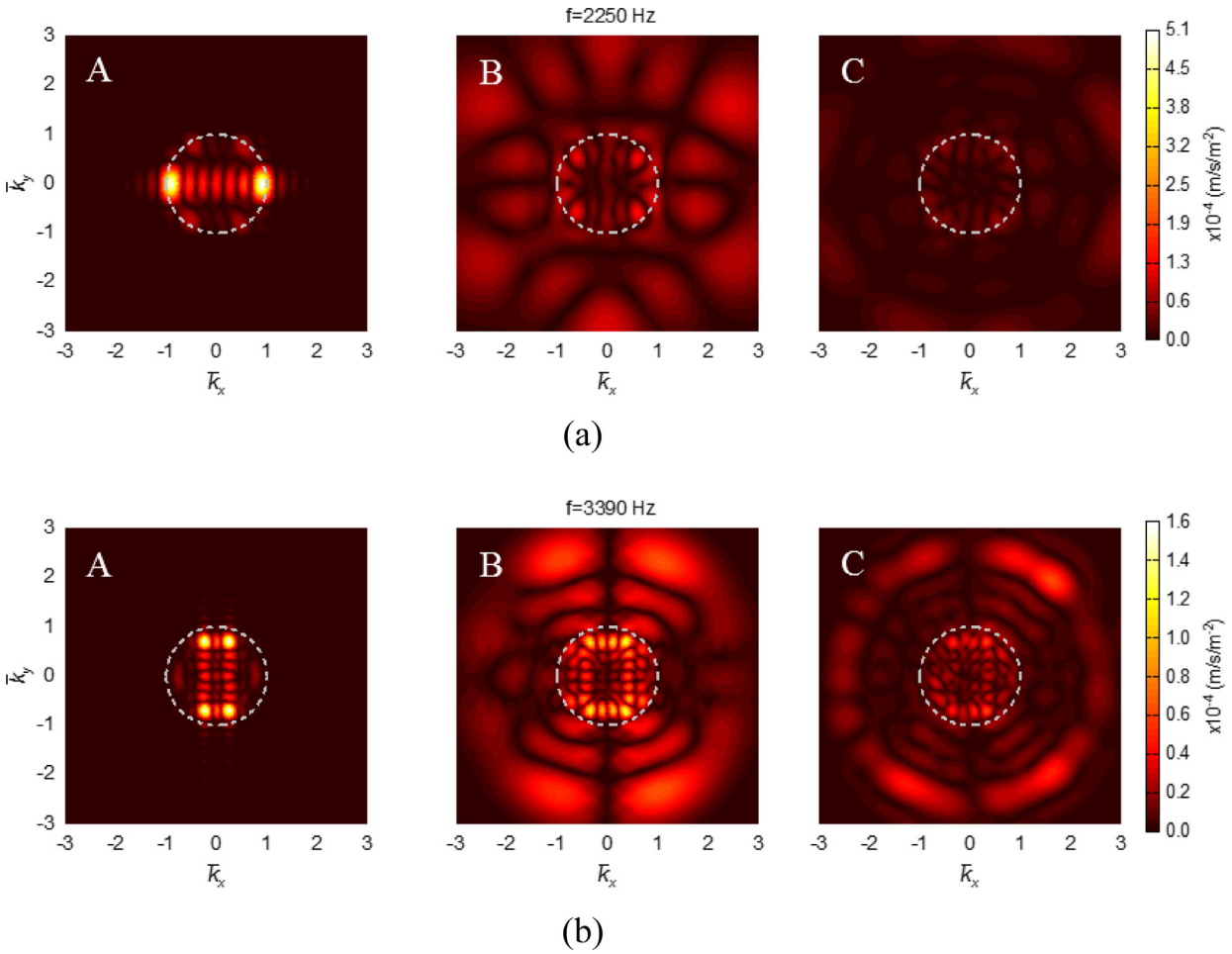

Fig. 14. Wavenumber spectra of uniform plates (A), standard ABH plates (B) and optimized ABH plates (C) at different frequencies: (a) 2250 Hz; (b) 3390 Hz. The dash circle indicates the corresponding normalized radiation circle with radius of $r = 1$.

change the so-called cut-on frequency [7] of the plate. In this sense, we would not expect a systematic improvement at low frequencies.

To better evaluate the global improvement on sound radiation, sound power results above the critical frequency are averaged into one-third octave bands and shown in Fig. 13. It can be seen that the averaged sound power is reduced by 1.5–2 dB in the frequency bands centered at 2500 Hz, 3150 Hz, 4000 Hz and 5000 Hz. The reduction of the sound power observed is attributed to the reduction in the vibration response and the radiation efficiency shown in Fig. 13(b). Additionally, the calculated radiation efficiency in the last four frequency bands are evidently reduced, which is justifiable considering the constraints in Eq. (4). Another explanation of the reduced radiation efficiency is due to the weakened stiffness of the plate; which can be seen from the reduced eigen-frequencies (not shown here).

It is relevant to reiterate that, although the dominant modes in the extended frequency range (above the 100 modes used in the optimization) were not directly used in the optimization, the achieved ABH profile does embrace the basic ABH features so that they play out even more systematically when frequency gets higher, as one might expect for an ABH structure.

As a final assessment, wavenumber transform analyses are carried out for the illustration of the improved ABH effect of the optimized ABH plate. To this end, spatial distributions of the vibration velocity are transformed into wavenumber domain. Same as before, the uniform plate is used as comparison basis. Comparisons between the uniform plate, plates with standard ABH profile and the optimized one are conducted at representative frequencies (2250 Hz around the critical frequency and 3390 Hz above the critical frequency) with results shown in Fig. 14.

Fig. 14(a) shows the vibration velocity distribution in the wavenumber domain at 2250 Hz. It can be seen that, for the uniform plate, vibration response of high amplitude mainly locates at the periphery of the normalized unit radiation circle. As to the standard ABH plate, vibration response inside the normalized unit radiation circle is reduced, as expected. A further reduction in vibration response of supersonic components is observed for the optimized ABH plate. Similarly,

Fig. 14(b) compares the vibration velocity at 3390 Hz, which is above the critical frequency of 1995 Hz. For the uniform plate, the vibration response of high amplitude resides inside the normalized unit radiation circle, as expected. However, for the standard and the optimized ABH plate, vibration response of supersonic components is reduced, and vibration response of high amplitude also spreads outside the normalized radiation circle. Compared with the standard ABH plate, the optimized one shows a reduction in vibration response of supersonic components inside the radiation circle. These analyses confirm the improved ABH effects of the optimized ABH plate in terms of sound radiation.

4. Conclusions

This paper reports an alternative ABH thickness profile in a plate through an optimization procedure by using the fast and elitist nondominated sorting genetic algorithm II in conjunction with a 2D semi-analytical Daubechies wavelet model. Maximization of the structural damping is taken as the objective function. Performance comparisons between the standard and the optimized ABH plates are conducted to show the superiority of the latter in terms of the ABH effects, as reflected by the overall enhancement of the structural damping, and a general reduction of the major vibration and sound radiation metrics. Main conclusions are summarized as follows:

1) Different from the standard ABH profiles, an alternative ABH thickness profile is revealed. Embedded into a benchmark rectangular plate, the ABH structure with the optimized thickness profile entails improved ABH effects as compared to the standard one. More specifically, the overall loss factor of the optimized ABH plate, averaged over the first one-hundred modes (taken as the objective function), is increased by 39.5% in the present configuration studied, as compared with the standard one when using the same amount of damping materials.
2) The new ABH profile features an offsetting of its minimum thickness away from the indentation center, thus forming a ring-shaped area/plateau inside the indentation. Different from the standard ABH plate, the extended thin thickness plateau between the center and the outer boundary of the optimized ABH indentation enlarges the energy focusing area, thus generating bi-directional ABH effects through energy trapping from both sides (inbound waves from the ABH boundary and outbound waves reflected back from the indentation center). As a result, the local ABH $(\bar{n}, 1)$ and $(\bar{n}, 2)$ modes dominate the overall increase of the system damping.
3) Compared with the standard ABH plate, the optimized ABH plate also entails a reduction in the mean square velocity and the radiated sound power, amounting roughly to 1.7 dB and 2.5 dB, respectively in the investigated case. Meanwhile, a reduced sound radiation efficiency of the plate above its critical frequency is also observed. Wavenumber transform analyses confirm the reduced vibration response of the supersonic vibration components, which are mainly responsible for the far-field sound radiation.

As a final remark, it is relevant to recall that, though definitely possible, the objective of this work is not to maximize the overall damping of the structure through adjusting the layout of the damping layer. It can be surmised that, with the new ABH profile, whatever conventional means which can increase the overall structural damping in a standard ABH profile should also be applicable to the present case. So the reported improvement resulting from the new profile should be regarded as additional improvement on the top of what can be obtained on a standard ABH profile.

Credit author statement

L. MA carried out the entire numerical analyses and drafted the paper. L. CHENG supervised the work and revised the paper. H. DONG provided comments when finalizing the paper and gave suggestions to revise the paper. L. CHENG initiated the idea based on his prior work.

Declaration of Competing Interest

The authors declare that they have no known competing financial interests or personal relationships that could have appeared to influence the work reported in this paper.

Acknowledgements

Authors thank the Research Grant Council of the Hong Kong SAR (PolyU 152009/17E) and National Science Foundation of China (No. 11532006) for their support.

References

[1] V. Denis, F. Gautier, A. Pelat, J. Poittevin, Measurement and modelling of the reflection coefficient of an Acoustic Black Hole termination, J. Sound Vib. 349 (2015) 67–79.
[2] F. Gautier, J. Cuenca, V.V. Krylov, L. Simon, Experimental investigation of the acoustic black hole effect for vibration damping in elliptical plates, in: acoustics, Paris, 2008, pp. 3318.
[3] W. Huang, H. Ji, J. Qiu, L. Cheng, Wave energy focalization in a plate with imperfect two-dimensional acoustic black hole indentation, J. Vib. Acoust. 138 (2016) 061004.

[4] D.J. O'Boy, V.V. Krylov, Vibration of a rectangular plate with a central power-law profiled groove by the Rayleigh–Ritz method, Appl. Acoust. 104 (2016) 24–32.
[5] P.A. Feurtado, S.C. Conlon, Wavenumber transform analysis for acoustic black hole design, J. Acoust. Soc. Am. 140 (2016) 718–727.
[6] L. Zhao, F. Semperlotti, Embedded Acoustic Black Holes for semi-passive broadband vibration attenuation in thin-walled structures, J. Sound Vib. 388 (2017) 42–52.
[7] S.C. Conlon, J.B. Fahnline, F. Semperlotti, Numerical analysis of the vibroacoustic properties of plates with embedded grids of acoustic black holes, J. Acoust. Soc. Am. 137 (2015) 447–457.
[8] P.A. Feurtado, S.C. Conlon, An experimental investigation of acoustic black hole dynamics at low, mid, and high frequencies, J. Vib. Acoust. 138 (2016) 061002.
[9] L. Ma, L. Cheng, Sound radiation and transonic boundaries of a plate with an acoustic black hole, J. Acoust. Soc. Am. 145 (2019) 164–172.
[10] E.P. Bowyer, V.V. Krylov, Experimental study of sound radiation by plates containing circular indentations of power-law profile, Appl. Acoust. 88 (2015) 30–37.
[11] M.A. Mironov, Propagation of a flexural wave in a plate whose thickness decreases smoothly to zero in a finite interval, Sov. Phys. Acoust. 34 (1988) 318–319.
[12] L. Tang, L. Cheng, H. Ji, J. Qiu, Characterization of acoustic black hole effect using a one-dimensional fully-coupled and wavelet-decomposed semi-analytical model, J. Sound Vib 374 (2016) 172–184.
[13] L. Tang, L. Cheng, Enhanced Acoustic Black Hole effect in beams with a modified thickness profile and extended platform, J. Sound Vib. 391 (2017) 116–126.
[14] V.V. Krylov, F.J.B.S. Tilman, Acoustic 'black holes' for flexural waves as effective vibration dampers, J. Sound Vib. 274 (2004) 605–619.
[15] V.B. Georgiev, J. Cuenca, F. Gautier, L. Simon, V.V. Krylov, Damping of structural vibrations in beams and elliptical plates using the acoustic black hole effect, J. Sound Vib. 330 (2011) 2497–2508.
[16] A. Pelat, F. Gautier, S.C. Conlon, F. Semperlotti, The acoustic black hole: a review of theory and applications, J. Sound Vib. (2020) 115316.
[17] L. Ma, L. Cheng, Topological optimization of damping layout for minimized sound radiation of an acoustic black hole plate, J. Sound Vib. 458 (2019) 349–364.
[18] H. Wei, H. Ji, C. Tao, J. Qiu, Optimal design of the damping layer in plate with imperfect Acoustic Black Hole for wave energy dissipation, in: INTER-NOISE and NOISE-CON Congress and Conference Proceedings, Institute of Noise Control Engineering, 2019, pp. 7763–7771.
[19] K. Hook, J. Cheer, S. Daley, A parametric study of an acoustic black hole on a beam, J. Acoust. Soc. Am. 145 (2019) 3488–3498.
[20] C.A. McCormick, M.R. Shepherd, Design optimization and performance comparison of three styles of one-dimensional acoustic black hole vibration absorbers, J. Sound Vib. 470 (2020) 115164.
[21] L. Ma, S. Zhang, L. Cheng, A 2D Daubechies wavelet model on the vibration of rectangular plates containing strip indentations with a parabolic thickness profile, J. Sound Vib. 429 (2018) 130–146.
[22] P.A. Feurtado, S.C. Conlon, F. Semperlotti, A normalized wave number variation parameter for acoustic black hole design, J. Acoust. Soc. Am. 136 (2014) EL148–EL152.
[23] K. Deb, A. Pratap, S. Agarwal, T. Meyarivan, A fast and elitist multiobjective genetic algorithm: NSGA-II, IEEE T. Evolut. Comput. 6 (2002) 182–197.
[24] K. Deb, R.B. Agrawal, Simulated binary crossover for continuous search space, Complex Syst 9 (1995) 115–148.